Quantum Effects on Unconventional Pinch Point Singularities

Nils Niggemann,[1,2,3,*] Yasir Iqbal,[3] and Johannes Reuther[1,2,3]
[1]Dahlem Center for Complex Quantum Systems and Fachbereich Physik, Freie Universität Berlin, D-14195 Berlin, Germany
[2]Helmholtz-Zentrum Berlin für Materialien und Energie, D-14109 Berlin, Germany
[3]Department of Physics and Quantum Center for Diamond and Emergent Materials (QuCenDiEM), Indian Institute of Technology Madras, Chennai 600036, India

(Received 15 December 2022; revised 8 April 2023; accepted 24 April 2023; published 12 May 2023)

Fracton phases are a particularly exotic type of quantum spin liquids where the elementary quasiparticles are intrinsically immobile. These phases may be described by unconventional gauge theories known as tensor or multipolar gauge theories, characteristic for so-called type-I or type-II fracton phases, respectively. Both variants have been associated with distinctive singular patterns in the spin structure factor, such as multifold pinch points for type-I and quadratic pinch points for type-II fracton phases. Here, we assess the impact of quantum fluctuations on these patterns by numerically investigating the spin $S = 1/2$ quantum version of a classical spin model on the octahedral lattice featuring exact realizations of multifold and quadratic pinch points, as well as an unusual pinch line singularity. Based on large scale pseudofermion and pseudo-Majorana functional renormalization group calculations, we take the intactness of these spectroscopic signatures as a measure for the stability of the corresponding fracton phases. We find that in all three cases, quantum fluctuations significantly modify the shape of pinch points or lines by smearing them out and shifting signal away from the singularities in contrast to effects of pure thermal fluctuations. This indicates possible fragility of these phases and allows us to identify characteristic fingerprints of their remnants.

DOI: 10.1103/PhysRevLett.130.196601

Introduction.—A particularly fascinating physical situation arises when a system of interacting spins realizes an emergent gauge theory, which is one of the defining properties of a quantum spin liquid [1]. Various different types of gauge theories may be realized in such phases. For example, quantum spin ice represents a variant of a quantum spin liquid, where an emergent U(1) gauge theory on a pyrochlore lattice establishes an astonishing analogy to three-dimensional electromagnetism including emergent photons and an effective fine-structure constant [2,3]. The key ingredient enabling these nontrivial properties is the gauge constraint that, in the charge-free sector of a U(1) gauge theory, takes the form of the Gauss law $\boldsymbol{\nabla} \cdot \boldsymbol{E}(\boldsymbol{r}) = 0$.

Meanwhile, generalizations of the standard U(1) gauge theories have become a new focus of theoretical investigations where the vector form of the Gauss law is replaced by a tensor structure [4–7], e.g., $\sum_{\mu\nu} \partial_\mu \partial_\nu E_{\mu\nu}(\boldsymbol{r}) = 0$, known as tensor gauge theories describing so-called fracton spin liquids [8,9]. The most remarkable consequence of this generalization is that, besides the effective charge of a quasiparticle, multipole moments of charges become conserved quantities giving rise to excitations with fractionalized mobility [10]. Two cases can be distinguished [11]: in type-I fracton phases [12–14], described by symmetric tensor gauge theories, the quasiparticles are either completely immobile or have a residual mobility along subdimensional manifolds. Otherwise, in type-II fracton phases [15–17] all quasiparticles are completely immobile. In the associated multipolar gauge theories the Gauss law contains derivatives of different orders restricting charge configurations to certain fractal patterns [18–21]. Remarkably, fracton phases also attract interest in fields such as quantum information [22,23] and high energy physics [24–27].

Recently, important steps have been undertaken to bring the rather abstract theoretical research on fracton phases closer to the established field of quantum magnetism and to experiments. For example, it has been found that type-I fracton phases manifest themselves in multifold pinch points [6] in the spin structure factor [Fig. 2(a)], generalizing the famous twofold pinch points known from conventional U(1) spin liquids [Fig. 1(c)]. Likewise, type-II fracton phases have been argued to be associated with quadratic pinch points [Fig. 3(d)] where contour lines exhibit a characteristic parabolic shape [28]. On a different front, a class of simple classical spin models has been identified [29] that gives straightforward access to classical spin liquids described by tensor gauge theories and to unconventional pinch points in the spin structure factor. However, it is an open but experimentally relevant question as to how stable these phases are under modification from the ideal situations in which they are defined, e.g., by allowing for quantum fluctuations.

In this Letter, we study the effects of quantum fluctuations on the ground state and finite-temperature phases of the classical spin model in Ref. [29]—the so-called

octochlore model—whose three dimensional octahedral lattice is realized in rare-earth antiperovskites [30,31]. This model represents a showcase example for exotic classical spin liquids: apart from known twofold and multifold pinch points we identify exact realizations of quadratic pinch points [28] as well as unconventional pinch line singularities [32]. We add quantum fluctuations to the system by promoting it from a classical ($S \to \infty$) to a quantum $S = 1/2$ Heisenberg model that is then numerically treated via two powerful quantum many-body techniques: the pseudofermion and the pseudo-Majorana functional renormalization group. Overall, we find that exotic pinch point features are drastically affected by quantum fluctuations and appear more fragile compared to conventional twofold pinch points.

Unconventional gauge theories from an octochlore model.—The octahedral lattice consists of corner-sharing octahedra and is defined by simple cubic lattice vectors $\boldsymbol{a}_m \in \{(1,0,0),(0,1,0),(0,0,1)\}$ together with a three site basis $\boldsymbol{b}_m = \boldsymbol{a}_m/2$. The Hamiltonian of the octochlore model [29] is constructed as the sum of squared vectors $\boldsymbol{M}_{\mathrm{oct},\alpha\beta}$ over all elementary octahedra:

$$H = \frac{J}{2}\sum_{\mathrm{oct}} \boldsymbol{M}^2_{\mathrm{oct},\alpha\beta}, \tag{1}$$

where $\boldsymbol{M}_{\mathrm{oct},\alpha\beta}$ is the sum of spins in a cluster, weighted by dimensionless parameters α, β:

$$\boldsymbol{M}_{\mathrm{oct},\alpha\beta} = \sum_{i\in\mathrm{oct}} \boldsymbol{S}_i + \alpha \sum_{i\in\langle\mathrm{oct}\rangle} \boldsymbol{S}_i + \beta \sum_{i\in\langle\langle\mathrm{oct}\rangle\rangle} \boldsymbol{S}_i. \tag{2}$$

Here, a reference octahedron "oct" is given by the green sites in Fig. 1(a), while its closest surrounding sites "$\langle$oct$\rangle$" and further distant sites "$\langle\langle$oct$\rangle\rangle$" are colored blue and cyan, respectively. Henceforth, we set the energy scale such that the maximal Heisenberg coupling between two spins is equal to one.

For classical spins $\boldsymbol{S}_i$, the system's extensively degenerate ground states follow from the constraints $\boldsymbol{M}_{\mathrm{oct},\alpha\beta} = 0$ that constitute discrete versions of Gauss's law. These constraints can be expressed in reciprocal space as $\sum_m L_m(\boldsymbol{q})\boldsymbol{S}_m(\boldsymbol{q}) = 0$ [29], where $m = 1, 2, 3$ label the sublattices, $\boldsymbol{S}_m(\boldsymbol{q})$ is the Fourier-transformed spin on sublattice m, and $L_m(\boldsymbol{q})$ is the mth component of the so-called constraint vector. Normalized constraint vectors $\tilde{L}_m(\boldsymbol{q}) = L_m(\boldsymbol{q})/\sqrt{\sum_n [L_n(\boldsymbol{q})]^2}$ can be defined over the entire $\boldsymbol{q}$ space except at singular points $\boldsymbol{q}^\star$ where $L_m(\boldsymbol{q}^\star) = 0$ for all m. For isolated points $\boldsymbol{q}^\star$ in momentum space and with $\tilde{L}_m(\boldsymbol{q})$ defined on the unit sphere S^2 one can assign a topological index to the defect configuration $\tilde{L}_m(\boldsymbol{q})$ around $\boldsymbol{q}^\star$ defined by the second homotopy group of S^2, which is the Skyrmion number Q [33,34]. As demonstrated in Ref. [29] nontrivial $Q \neq 0$ give rise to pinch points at $\boldsymbol{q} = \boldsymbol{q}^\star$ in the equal-time

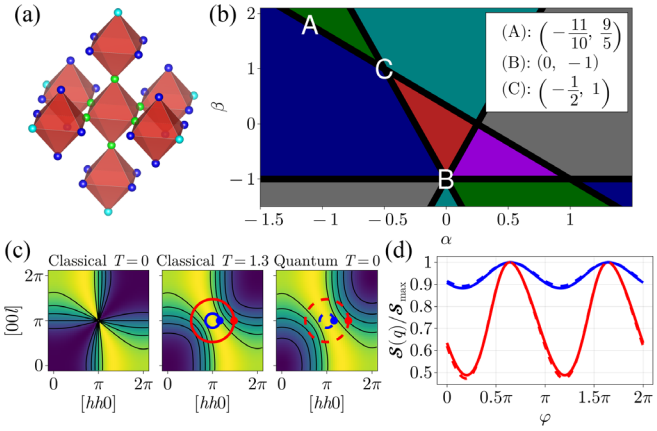

FIG. 1. (a) Octochlore model: differently weighted sites in Eq. (2) are indicated by different colors. (b) Phase diagram of the model from Ref. [29]. The labels A, B, C [with parameters (α,β) given in the inset] indicate the locations of multifold pinch points, quadratic pinch points, and pinch lines as shown in Figs. 2–4, respectively. (c) Spin structure factor of a twofold pinch point at $\alpha = \beta = 0$ for the classical and quantum model. (d) Spin structure factor $\mathcal{S}(\boldsymbol{q})$ along circular paths indicated in (c) normalized to their maxima.

spin structure factor $\mathcal{S}(\boldsymbol{q}) \equiv \langle \boldsymbol{S}(-\boldsymbol{q}) \cdot \boldsymbol{S}(\boldsymbol{q})\rangle$, where $|Q| = 1$ is associated with twofold pinch points. Furthermore, expanding $L_m(\boldsymbol{q})$ in powers of $\boldsymbol{q}$ around $\boldsymbol{q}^\star$ reveals the underlying continuum gauge theory.

The number of such defects and their arrangement in the Brillouin zone yields a phase diagram spanned by α and β featuring 10 distinct classical spin liquids; see Fig. 1(b). In particular, at points along the boundary [i.e., point A in Fig. 1(b)] multiple defects with $Q = \pm 1$ merge, leading to a higher $|Q| > 1$ associated with a tensor gauge theory and multifold pinch points; see Ref. [29]. In addition, we have identified even richer phenomena at crossing points of several phase boundaries: point B in Fig. 1(b) displays a pinch point with purely parabolic contours, recently predicted to be a hallmark signature of type-II fracton phases [28], while point C features unusual, one-dimensional manifolds of pinch points, so-called pinch-lines [32].

Methods.—The classical model in Eq. (1) is treated within a standard large-N approach [35], both at zero and finite temperatures, previously found to correctly capture the qualitative behavior for this system [29]. To study the vastly more complicated quantum $S = 1/2$ version, we employ two functional renormalization group (FRG) approaches that replace spin operators by fermionic pseudoparticles. An established approach at zero temperature is the so-called pseudofermion FRG (PF-FRG) [36–42], in which spin $S = 1/2$ operators are mapped onto two flavors of complex fermions $f_{i\uparrow}, f_{i\downarrow}$ as $S_i^\mu = \frac{1}{2}\sum_{a,b\in\{\uparrow,\downarrow\}} f^\dagger_{ia}\sigma^\mu_{ab} f_{ib}$. At finite temperatures, we apply the pseudo-Majorana FRG (PM-FRG), where we, instead, represent spins by three flavors $\mu = x, y, z$ of SO(3)-symmetric Majorana fermions $\{\eta_i^\mu, \eta_j^\nu\} = \delta_{ij}\delta_{\mu\nu}$ as $S_i^\mu = -(i/2)\sum_{\nu,\sigma}\epsilon_{\mu\nu\sigma}\eta_i^\nu\eta_i^\sigma$, without

introducing unphysical states [43–45]. For both approaches, the resulting interacting model is treated in the thermodynamic limit [46] using one-loop FRG. Here, $\sim 10^8$ first order ordinary differential equations are solved numerically as a function of an artificial Matsubara frequency cutoff Λ. In the physical limit $\Lambda \to 0$, we obtain renormalized fermionic vertex functions well beyond mean field, from which we calculate the equal-time spin structure factor $\mathcal{S}(\boldsymbol{q})$. Despite the common FRG background, the approximations associated with a one-loop scheme are different in both approaches such that one can consider the PF-FRG and PM-FRG as independent and complementary techniques. Still, we observe excellent agreement between the equal-time PM-FRG structure factor for the lowest simulated temperatures with the one obtained from PF-FRG at $T = 0$ [46].

Twofold pinch points.—Even though not the focus of this work, we start with a brief discussion of more conventional twofold pinch points with $|Q| = 1$, occurring in the bulk of every phase of Fig. 1(b). At the pinch point positions $\boldsymbol{q} = \boldsymbol{q}^\star$, the lowest nonvanishing term in an expansion of $L_m(\boldsymbol{q})$ is the linear one, and hence, the emergent continuum Gauss law has the linear form $\boldsymbol{\nabla} \cdot \boldsymbol{E}(\boldsymbol{r}) = \boldsymbol{q} \cdot \boldsymbol{E}(\boldsymbol{q}) = 0$ where $\boldsymbol{E}(\boldsymbol{q}) = \sum_m S^z_m(\boldsymbol{q}) \partial_{\boldsymbol{q}} L_m(\boldsymbol{q})$ [47]. Under the influence of quantum fluctuations at $T = 0$ in the $S = 1/2$ case treated with PF-FRG, twofold pinch points show the typical broadening illustrated in Fig. 1(c) for the case $\alpha = \beta = 0$, while the overall pinch point shape stays rather intact. In particular, we observe the effects of quantum fluctuations to be analogous to those at a finite temperature $T \sim 1.3$. This broadening indicates violations of the ice rule constraint, and is expected as the absolute spin magnitudes $\boldsymbol{M}^2_{\mathrm{oct},\alpha\beta}$ of neighboring octahedra do not mutually commute and thus fluctuate, i.e., $\langle \boldsymbol{M}^2_{\mathrm{oct},\alpha\beta} \rangle \neq 0$. Importantly, the signal at $\boldsymbol{q} = \boldsymbol{q}^\star$ remains strong and no indications for magnetic long-range order are observed in the full α-β plane [46,48]. We find these observations to be in direct analogy with past studies of the closely related nearest neighbor pyrochlore Heisenberg model [41,44,49–56].

Multifold pinch points.—A vanishing linear term in an expansion of $L_m(\boldsymbol{q})$ around $\boldsymbol{q} = \boldsymbol{q}^\star$ is associated with multifold pinch points [6,7,29]. An instructive example occurs at $\alpha = -11/10$, $\beta = 9/5$, and $\boldsymbol{q}^\star = (\pi, \pi, \pi)$, with a topological index $Q = -7$ and six lobes of large intensity in the hhl plane; see Fig. 2(a) and Ref. [29]. We identify a gauge constraint of third rank $\sum_{\mu\nu\sigma} q_\mu q_\nu q_\sigma E_{\mu\nu\sigma}(\boldsymbol{q}) = 0$ where $E_{\mu\nu\rho}(\boldsymbol{q}) = \sum_m S^z_m(\boldsymbol{q}) \partial_{q_\mu} \partial_{q_\nu} \partial_{q_\rho} L_m(\boldsymbol{q})$, implying conserved scalar charge, dipole and quadrupole moments. Figure 2 shows the impact of both quantum and thermal fluctuations on this multifold pinch point.

The value of $\mathcal{S}(\boldsymbol{q})$ along circular paths around the pinch point illustrates the presence of the singularity: for the exact gauge theory in the classical $T = 0$ model, it retains the same strong angular dependence for arbitrarily small radii; see Fig. 2(e). Thermal fluctuations induce a rather featureless broadening and the angular dependence of the signal

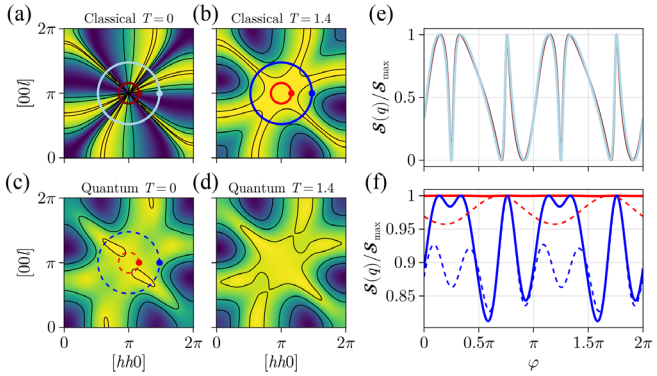

FIG. 2. (a)–(d) Spin structure factor $\mathcal{S}(\boldsymbol{q})$ in the hhl plane for a multifold $Q = -7$ pinch point found at location A ($\alpha = -\frac{11}{10}$, $\beta = \frac{9}{5}$) in the phase diagram of Fig. 1. (e) $\mathcal{S}(\boldsymbol{q})$ for the two paths indicated in (a), normalized to its maximum value along each path. (f) As in (e) but comparing classical thermal and quantum fluctuations along the paths in (b) and (c). The paths are counterclockwise and the start point $\varphi = 0$ is indicated by a marker.

vanishes at small distances from the pinch point; see full red line in Fig. 2(f). Interestingly, the effects of quantum fluctuations are very different. In addition to a broadening, quantum fluctuations add a shift of spectral weight away from the pinch point origin in favor of soft maxima at incommensurate positions, effectively tearing apart the pinch point. We note that this observation stands in stark contrast to the case of twofold pinch points shown in Fig. 1(c), for which quantum fluctuations appear to act similarly to thermal ones.

In order to physically interpret the data in Fig. 2, two types of quantum effects need to be distinguished. First, the aforementioned broadening of pinch points rather indicates the destruction of the underlying gauge theory. However, a second well-known quantum effect consistent with a gauge theory is the formation of gapless photon modes with dispersion $\omega(\boldsymbol{q})$, resulting from an emergent conjugate vector potential $A(\boldsymbol{r})$. These photon modes give rise to an extra factor $\omega(\boldsymbol{q})$ in the spin structure factor [i.e., $\mathcal{S}(\boldsymbol{q}) \to \omega(\boldsymbol{q})\mathcal{S}(\boldsymbol{q})$] suppressing the signal at the singularity due to $\omega(\boldsymbol{q}^\star) = 0$ [6,28,57]. To test whether the weight distribution in Fig. 2(c) contains possible signatures of such a modulation, we note that the mere multiplication of an exact pinch point with an isotropic factor $\omega(\boldsymbol{q}) \sim |\boldsymbol{q} - \boldsymbol{q}^\star|^\gamma$ [or, for that matter, *any* function $\omega(|\boldsymbol{q} - \boldsymbol{q}^\star|)$] [58] leaves the singularity intact such that $\mathcal{S}(\boldsymbol{q})$ along rings around the pinch point, normalized to its maximum on each path, would remain unchanged upon decreasing the radius of the rings. However, the dashed red and blue graphs in Fig. 2(f) illustrating the normalized signal along the ringlike paths in Fig. 2(c) are qualitatively very different and, hence, our results seem incompatible with an emergent photon mode. While it is possible that the ground state is described by a different gauge theory (i.e., with an emergent electric field

given by a more complex function of spin operators), we deem it questionable whether fractonic phenomena that have been associated with these spectroscopic features still occur in the $S = 1/2$ limit of the Heisenberg model.

Quadratic pinch points.—A further generalization occurs if the gauge constraint contains derivatives of different orders as is characteristic for multipolar gauge theories describing type-II fracton phases. This gives rise to quadratic pinch points in the spin structure factor where lobes of strong intensity follow contour lines of the form $q_\parallel \propto a q_\perp^2$ with $q_\parallel$ and $q_\perp$ being two perpendicular momentum space directions and a is the lattice constant (which is set to 1 here). The mixing of derivatives causes the lattice constant to explicitly appear in these spectroscopic patterns, which is a direct manifestation of the ultraviolet-infrared mixing described in recent literature [28].

Strikingly, we have identified such quadratic pinch points in the classical octochlore model at $\alpha = 0$, $\beta = -1$, and $\boldsymbol{q}^\star = (0, 0, \pi)$. The effective gauge theory in this case contains first derivatives along the z direction, as $\partial_{q_z} L_3(\boldsymbol{q}) \neq 0$, while for the perpendicular x, y directions $\partial_{q_x} L_m(\boldsymbol{q}) = \partial_{q_y} L_m(\boldsymbol{q}) = 0$ for $m = 1, 2, 3$ and the lowest nonvanishing contribution comes from second derivatives. The resulting quadratic pinch point in classical large N [Fig. 3(d)] has a shape that is similar to predictions from the U(1) Haah code [28]. The effect of finite temperatures in large N only amounts to a broadening near $\boldsymbol{q}^\star$ while retaining the quadratic shape and the strong signal around $\boldsymbol{q}^\star$. This is to be contrasted with PM-FRG at the same temperature where the signal is reduced near $\boldsymbol{q}^\star$ and quadratic contours are no longer discernible. This trend continues down to $T = 0$ where the spin-structure factor appears even more strongly reduced around $\boldsymbol{q}^\star$. Again

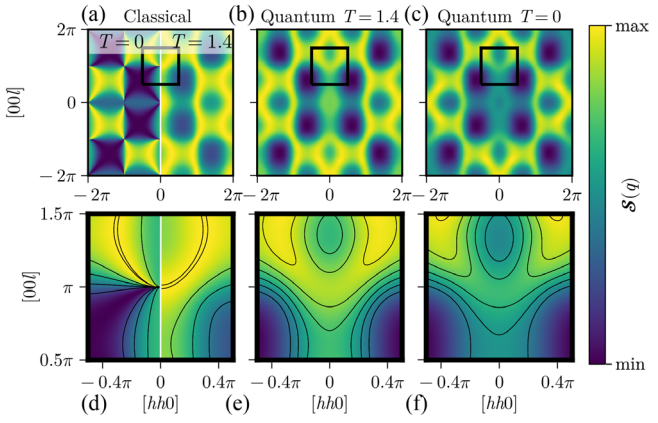

FIG. 3. Pinch point with parabolic contours in the hhl plane found at point B ($\alpha = 0$, $\beta = -1$). (a) Classical large-N result for temperatures $T = 0$ (left half) and $T = 1.4$ (right half). (b) Quantum model at $T = 1.4$ and (c) at $T = 0$ obtained from PM-FRG and PF-FRG in the low cutoff limit, respectively. (d)–(f) Magnifications of the regions indicated by black squares in the upper panel together with black contour lines.

however, this result seems incompatible with emergent photons; see Ref. [46].

As a side remark, the model with $\alpha = 0$, $\beta = -1$ also hosts a fourfold pinch point [7]; see Fig. 3(a) at $\boldsymbol{q}^\star = \boldsymbol{0}$, associated with a trace-full rank-2 tensor gauge constraint. With the observed reduction of $\mathcal{S}(\boldsymbol{q})$ and the formation of a local minimum at $\boldsymbol{q}^\star = \boldsymbol{0}$ in the quantum model as $T \to 0$, this is another example reflecting the strong impact of quantum fluctuations on exotic pinch points.

Pinch lines.—Points $\boldsymbol{q}^\star$ of vanishing constraint vector are not necessarily isolated in momentum space but can form one-dimensional manifolds. This situation has previously been studied in Ref. [32] where the phenomenon has been dubbed a pinch line. Such patterns exhibit conventional twofold pinch points in all planar cuts through the pinch line. For the classical pyrochlore model investigated in Ref. [32] an underlying gauge constraint linear in the derivatives but with a tensor structure has been identified and a possible relevance for the pyrochlore material $Tb_2Ti_2O_7$ [59] has been pointed out.

We have found an analogous feature in the octochlore model at $\alpha = -\frac{1}{2}$ and $\beta = 1$ where pinch lines run along [111] and symmetry related directions in momentum space. The lowest nonvanishing derivatives of $L_m(\boldsymbol{q})$ at $\boldsymbol{q}^\star$ are first order derivatives perpendicular to the pinch lines, in agreement with the pyrochlore model of Ref. [32]. Since the topological defect is now linelike and observing that the normalized constraint vector $\tilde{L}_m(\boldsymbol{q})$ avoids two opposite points on the unit sphere S^2 [46], the topological index is given by the integer vortex winding number w. We find $|w| = 1$ and consequently, twofold pinch points in planar cuts through the line defect; see bottom panel of Fig. 4 depicting cuts at $q_z = 0.5\pi$. Thermal fluctuations in the classical model [Fig. 4(a), right] shift spectral weight toward the pinch lines such that they become visible in

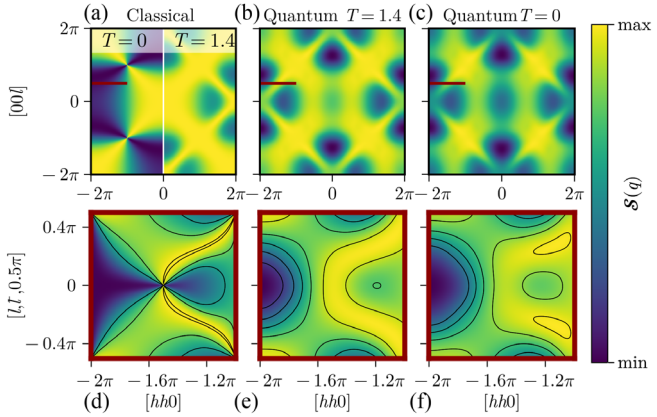

FIG. 4. (a)–(c) Temperature dependent spin structure factor for a pinch line at $\alpha = -\frac{1}{2}$, $\beta = 1$ [C in Fig. 1(b)] in the [111] direction. Panels (d)–(f) show a cut through the pinch line, here given by $q_z = 0.5\pi$ as indicated by the solid dark red line in panels (a)–(c).

the *hhl* plane as well-defined, broadened lines of constant strong signal.

For the corresponding quantum model, similar observations to the previous cases can be made, such as a redistribution of spectral weight away from the pinch line when temperature is lowered, as shown in the bottom panel of Fig. 4. It is again worth contrasting this behavior with conventional twofold pinch points representing isolated point defects where quantum fluctuations are not seen to significantly reduce the signal at $\boldsymbol{q} = \boldsymbol{q}^\star$; see the example in Fig. 1(c).

Discussion.—We have identified the classical octochlore model as an exquisite physical platform for studying exotic spectroscopic features, such as multifold and quadratic pinch points as well as pinch lines, all associated with unconventional gauge theories. Numerical studies that systematically investigate the impact of quantum fluctuations on the corresponding classical spin liquids are, however, lacking so far. In our endeavor to fill this gap, we treat the quantum spin $S = 1/2$ model employing state-of-the-art PF-FRG and PM-FRG methods. We find a recurring theme in our results: multifold pinch points, quadratic pinch points, and pinch lines all undergo a significantly different modification under quantum fluctuations than conventional twofold pinch points, showing a reduction of $\mathcal{S}(\boldsymbol{q})$ at $\boldsymbol{q}^\star$ that is also at variance compared to the effects of pure thermal fluctuations in the classical case. This also implies that the absence of unconventional pinch points in an experimentally measured spin structure factor does not necessarily exclude the realization of a higher-rank $U(1)$ gauge theory in the corresponding classical system.

From a methodological perspective, here, we benefit from the fact that our octochlore model has SU(2) spin symmetry that simplifies the application of PF-FRG and PM-FRG enormously. A (numerically more challenging) continuation of our present work could be to lift the SU(2) symmetry by considering an Ising version of the octochlore model supplemented with small transverse couplings, thus realizing an analogous situation as in quantum spin ice models. This will help identifying the fate of exotic pinch point singularities along a continuous classical-to-quantum interpolation. Thus, our results strongly motivate new avenues in the investigations of these exotic pinch points under quantum fluctuations, which appear to have a more significant impact compared to twofold pinch points. Furthermore, our work sets the stage for determining the microscopic wave functions describing these resulting quantum phases, and whose correlation functions give rise to the static structure factors obtained here [60].

We thank Owen Benton and Roderich Moessner for insightful discussions. N. N. and J. R. acknowledge support from the Deutsche Forschungsgemeinschaft (DFG, German Research Foundation), within Project-ID 277101999 CRC 183 (Project A04). N. N. thanks IIT Madras for funding a three-month stay through an International Graduate Student Travel award that facilitated completion of this research work. J. R. thanks IIT Madras for a Visiting Faculty Fellow position under the IoE program during which part of the research work and manuscript writing were carried out. Y. I. acknowledges support from DST, India through MATRICS Grant No. MTR/2019/001042, CEFIPRA Project No. 64T3-1, ICTP through the Associates Programme and from the Simons Foundation through Grant No. 284558FY19. This research was supported in part by the National Science Foundation under Grant No. NSF PHY-1748958, IIT Madras through the Institute of Eminence (IoE) program for establishing the QuCenDiEM group (Project No. SP22231244CPMOEXQCDHOC), the International Centre for Theoretical Sciences (ICTS), Bengaluru, India during a visit for participating in the program "Frustrated Metals and Insulators" (Code: ICTS/frumi2022/9). N. N. acknowledges usage of the JUWELS cluster at the Forschungszentrum Jülich and the Noctua2 cluster at the Paderborn Center for Parallel Computing (PC^2). Y. I. acknowledges the use of the computing resources at HPCE, IIT Madras.

*Corresponding author.
nils.niggemann@fu-berlin.de

[1] L. Savary and L. Balents, Quantum spin liquids: a review, Rep. Prog. Phys. **80**, 016502 (2016).
[2] M. Hermele, M. P. A. Fisher, and L. Balents, Pyrochlore photons: The $U(1)$ spin liquid in a $S = \frac{1}{2}$ three-dimensional frustrated magnet, Phys. Rev. B **69**, 064404 (2004).
[3] S. D. Pace, S. C. Morampudi, R. Moessner, and C. R. Laumann, Emergent Fine Structure Constant of Quantum Spin Ice Is Large, Phys. Rev. Lett. **127**, 117205 (2021).
[4] C. Xu, Gapless bosonic excitation without symmetry breaking: An algebraic spin liquid with soft gravitons, Phys. Rev. B **74**, 224433 (2006).
[5] M. Pretko, Subdimensional particle structure of higher rank $U(1)$ spin liquids, Phys. Rev. B **95**, 115139 (2017).
[6] A. Prem, S. Vijay, Y.-Z. Chou, M. Pretko, and R. M. Nandkishore, Pinch point singularities of tensor spin liquids, Phys. Rev. B **98**, 165140 (2018).
[7] H. Yan, O. Benton, L. D. C. Jaubert, and N. Shannon, Rank–2 $U(1)$ Spin Liquid on the Breathing Pyrochlore Lattice, Phys. Rev. Lett. **124**, 127203 (2020).
[8] R. M. Nandkishore and M. Hermele, Fractons, Annu. Rev. Condens. Matter Phys. **10**, 295 (2019).
[9] M. Pretko, X. Chen, and Y. You, Fracton phases of matter, Int. J. Mod. Phys. A **35**, 2030003 (2020).
[10] M. Pretko, Generalized electromagnetism of subdimensional particles: A spin liquid story, Phys. Rev. B **96**, 035119 (2017).
[11] S. Vijay, J. Haah, and L. Fu, Fracton topological order, generalized lattice gauge theory, and duality, Phys. Rev. B **94**, 235157 (2016).
[12] C. Chamon, Quantum Glassiness in Strongly Correlated Clean Systems: An Example of Topological Overprotection, Phys. Rev. Lett. **94**, 040402 (2005).

[13] S. Bravyi, B. Leemhuis, and B. M. Terhal, Topological order in an exactly solvable 3D spin model, Ann. Phys. (N.Y.) **326**, 839 (2011).

[14] S. Vijay, J. Haah, and L. Fu, A new kind of topological quantum order: A dimensional hierarchy of quasiparticles built from stationary excitations, Phys. Rev. B **92**, 235136 (2015).

[15] J. Haah, Local stabilizer codes in three dimensions without string logical operators, Phys. Rev. A **83**, 042330 (2011).

[16] B. Yoshida, Exotic topological order in fractal spin liquids, Phys. Rev. B **88**, 125122 (2013).

[17] C. Castelnovo and C. Chamon, Topological quantum glassiness, Philos. Mag. **92**, 304 (2012).

[18] D. Bulmash and M. Barkeshli, Generalized $U(1)$ Gauge Field Theories and Fractal Dynamics, arXiv:1806.01855v1.

[19] A. T. Schmitz, Distilling Fractons from Layered Subsystem-Symmetry Protected Phases, arXiv:1910.04765v1.

[20] A. Gromov, Towards Classification of Fracton Phases: The Multipole Algebra, Phys. Rev. X **9**, 031035 (2019).

[21] A. Gromov, A Duality Between U(1) Haah Code and 3D Smectic A Phase, arXiv:2002.11817v1.

[22] B. M. Terhal, Quantum error correction for quantum memories, Rev. Mod. Phys. **87**, 307 (2015).

[23] A. T. Schmitz, H. Ma, R. M. Nandkishore, and S. A. Parameswaran, Recoverable information and emergent conservation laws in fracton stabilizer codes, Phys. Rev. B **97**, 134426 (2018).

[24] H. Yan, Hyperbolic fracton model, subsystem symmetry, and holography, Phys. Rev. B **99**, 155126 (2019).

[25] H. Yan, Hyperbolic fracton model, subsystem symmetry, and holography. II. The dual eight-vertex model, Phys. Rev. B **100**, 245138 (2019).

[26] N. Seiberg and S.-H. Shao, Exotic $U(1)$ symmetries, duality, and fractons in $3+1$-dimensional quantum field theory, SciPost Phys. **9**, 046 (2020).

[27] P. Gorantla, H. T. Lam, N. Seiberg, and S.-H. Shao, fcc lattice, checkerboards, fractons, and quantum field theory, Phys. Rev. B **103**, 205116 (2021).

[28] O. Hart and R. Nandkishore, Spectroscopic fingerprints of gapless type-II fracton phases, Phys. Rev. B **105**, L180416 (2022).

[29] O. Benton and R. Moessner, Topological Route to New and Unusual Coulomb Spin Liquids, Phys. Rev. Lett. **127**, 107202 (2021).

[30] S. R. Sklan and C. L. Henley, Nonplanar ground states of frustrated antiferromagnets on an octahedral lattice, Phys. Rev. B **88**, 024407 (2013).

[31] A. Szabó, F. Orlandi, and P. Manuel, Fragmented Spin Ice and Multi-k Ordering in Rare-Earth Antiperovskites, Phys. Rev. Lett. **129**, 247201 (2022).

[32] O. Benton, L. D. C. Jaubert, H. Yan, and N. Shannon, A spin-liquid with pinch-line singularities on the pyrochlore lattice, Nat. Commun. **7**, 11572 (2016).

[33] N. D. Mermin, The topological theory of defects in ordered media, Rev. Mod. Phys. **51**, 591 (1979).

[34] *Points, Lines and Walls in Liquid Crystals, Magnetic Systems and Various Ordered Media*, edited by M. Kléman (John Wiley & Sons Inc, New York, 1983).

[35] S. V. Isakov, K. Gregor, R. Moessner, and S. L. Sondhi, Dipolar Spin Correlations in Classical Pyrochlore Magnets, Phys. Rev. Lett. **93**, 167204 (2004).

[36] J. Reuther and P. Wölfle, J_1-J_2 frustrated two-dimensional Heisenberg model: Random phase approximation and functional renormalization group, Phys. Rev. B **81**, 144410 (2010).

[37] Y. Iqbal, R. Thomale, F. Parisen Toldin, S. Rachel, and J. Reuther, Functional renormalization group for three-dimensional quantum magnetism, Phys. Rev. B **94**, 140408(R) (2016).

[38] M. L. Baez and J. Reuther, Numerical treatment of spin systems with unrestricted spin length S: A functional renormalization group study, Phys. Rev. B **96**, 045144 (2017).

[39] F. L. Buessen, V. Noculak, S. Trebst, and J. Reuther, Functional renormalization group for frustrated magnets with nondiagonal spin interactions, Phys. Rev. B **100**, 125164 (2019).

[40] J. Thoenniss, M. K. Ritter, F. B. Kugler, J. V. Delft, and M. Punk, Multiloop pseudofermion functional renormalization for quantum spin systems: Application to the spin-$\frac{1}{2}$ kagome Heisenberg model, arXiv:2011.01268v1.

[41] D. Kiese, T. Müller, Y. Iqbal, R. Thomale, and S. Trebst, Multiloop functional renormalization group approach to quantum spin systems, Phys. Rev. Res. **4**, 023185 (2022).

[42] D. Roscher, F. L. Buessen, M. M. Scherer, S. Trebst, and S. Diehl, Functional renormalization group approach to $\mathrm{SU}(N)$ Heisenberg models: Momentum-space renormalization group for the large-n limit, Phys. Rev. B **97**, 064416 (2018).

[43] N. Niggemann, B. Sbierski, and J. Reuther, Frustrated quantum spins at finite temperature: Pseudo-Majorana functional renormalization group approach, Phys. Rev. B **103**, 104431 (2021).

[44] N. Niggemann, J. Reuther, and B. Sbierski, Quantitative functional renormalization for three-dimensional quantum Heisenberg models, SciPost Phys. **12**, 156 (2022).

[45] B. Schneider, D. Kiese, and B. Sbierski, Taming pseudofermion functional renormalization for quantum spins: Finite-temperatures and the Popov-Fedotov trick, Phys. Rev. B **106**, 235113 (2022).

[46] See Supplemental Material at http://link.aps.org/supplemental/10.1103/PhysRevLett.130.196601 for methodological details and a discussion on pinch points.

[47] Derivatives here are taken at $\boldsymbol{q}=\boldsymbol{q}^{\star}$ and $\boldsymbol{q}$ is meant to be the momentum relative to $\boldsymbol{q}^{\star}$. Furthermore, since the different spin components $\mu=x,\ y,\ z$ do not couple in the spin constraint, one may restrict to the z component without loss of generality.

[48] C. L. Henley, Power-law spin correlations in pyrochlore antiferromagnets, Phys. Rev. B **71**, 014424 (2005).

[49] Y. Iqbal, T. Müller, P. Ghosh, M. J. P. Gingras, H. O. Jeschke, S. Rachel, J. Reuther, and R. Thomale, Quantum and Classical Phases of the Pyrochlore Heisenberg Model with Competing Interactions, Phys. Rev. X **9**, 011005 (2019).

[50] R. Schäfer, I. Hagymási, R. Moessner, and D. J. Luitz, Pyrochlore $S=\frac{1}{2}$ Heisenberg antiferromagnet at finite temperature, Phys. Rev. B **102**, 054408 (2020).

[51] I. Hagymási, R. Schäfer, R. Moessner, and D. J. Luitz, Possible Inversion Symmetry Breaking in the $S=1/2$ Pyrochlore Heisenberg Magnet, Phys. Rev. Lett. **126**, 117204 (2021).

[52] N. Astrakhantsev, T. Westerhout, A. Tiwari, K. Choo, A. Chen, M. H. Fischer, G. Carleo, and T. Neupert, Broken-Symmetry Ground States of the Heisenberg Model on the Pyrochlore Lattice, Phys. Rev. X **11**, 041021 (2021).

[53] P. Müller, A. Lohmann, J. Richter, and O. Derzhko, Thermodynamics of the pyrochlore-lattice quantum Heisenberg antiferromagnet, Phys. Rev. B **100**, 024424 (2019).

[54] O. Derzhko, T. Hutak, T. Krokhmalskii, J. Schnack, and J. Richter, Adapting Planck's route to investigate the thermodynamics of the spin-half pyrochlore Heisenberg antiferromagnet, Phys. Rev. B **101**, 174426 (2020).

[55] M. Hering, V. Noculak, F. Ferrari, Y. Iqbal, and J. Reuther, Dimerization tendencies of the pyrochlore Heisenberg antiferromagnet: A functional renormalization group perspective, Phys. Rev. B **105**, 054426 (2022).

[56] R. Schäfer, B. Placke, O. Benton, and R. Moessner, Abundance of hard-hexagon crystals in the quantum pyrochlore antiferromagnet, arXiv:2210.07235v2.

[57] O. Benton, O. Sikora, and N. Shannon, Seeing the light: Experimental signatures of emergent electromagnetism in a quantum spin ice, Phys. Rev. B **86**, 075154 (2012).

[58] In the most common types of U(1) gauge theories including rank-1 and rank-2 versions the photon dispersion is linear, i.e., $\gamma = 1$, as long as charges are scalar [6].

[59] T. Fennell, M. Kenzelmann, B. Roessli, M. K. Haas, and R. J. Cava, Power-Law Spin Correlations in the Pyrochlore Antiferromagnet $Tb_2Ti_2O_7$, Phys. Rev. Lett. **109**, 017201 (2012).

[60] M. Hering, J. Sonnenschein, Y. Iqbal, and J. Reuther, Characterization of quantum spin liquids and their spinon band structures via functional renormalization, Phys. Rev. B **99**, 100405(R) (2019).